Research Article Vol. 57, No. 4 / February 1 2018 / Applied Optics 573

applied optics

Evaluation of the communication quality of free-space laser communication based on the power-in-the-bucket method

Xianghui Yin,[1,2] Rui Wang,[1,2] Shaoxin Wang,[1] Yukun Wang,[1] Chengbin Jin,[1,2] Zhaoliang Cao,[1,*] and Li Xuan[1]

[1]State Key Laboratory of Applied Optics, Changchun Institute of Optics, Fine Mechanics and Physics, Chinese Academy of Sciences, 130033 Changchun, Jilin, China
[2]University of Chinese Academy of Sciences, Beijing 100049, China
*Corresponding author: caozlok@ciomp.ac.cn

Received 6 October 2017; revised 15 December 2017; accepted 18 December 2017; posted 19 December 2017 (Doc. ID 308712); published 23 January 2018

Atmospheric turbulence seriously affects the quality of free-space laser communication. The Strehl ratio (SR) is used to evaluate the effect of atmospheric turbulence on the receiving energy of free-space laser communication systems. However, the SR method does not consider the area of the laser-receiving end face. In this study, the power-in-the-bucket (PIB) method is demonstrated to accurately evaluate the effect of turbulence on the receiving energy. A theoretical equation is first obtained to calculate PIB. Simulated and experimental validations are then performed to verify the effectiveness of the theoretical equation. This work may provide effective guidance for the design and evaluation of free-space laser communication systems.

OCIS codes: (060.2605) Free-space optical communication; (010.1290) Atmospheric optics; (010.3310) Laser beam transmission; (010.0010) Atmospheric and oceanic optics.

https://doi.org/10.1364/AO.57.000573

1. INTRODUCTION

Free-space laser communication has been widely investigated because of its high bandwidth and anti-interference performance [1–5]. Many communication modes, such as horizontal, space-based, and satellite-to-Earth link, have been developed. Communication quality will be affected by atmospheric turbulence for certain communication modes, such as satellite-to-Earth link and horizontal laser communication. Therefore, the effect of atmospheric turbulence on free-space laser communication has been analyzed by numerous researchers. Tyson *et al.* investigated the effects of low-order aberrations on the bit error rate (BER) model from the scintillation probability [6]. Liu *et al.* studied the effect of atmospheric turbulence on the coherent efficiency of coherent communication [7]. For single-mode fiber reception, Ruilier established a mode-coupling theory to evaluate the effect of atmospheric turbulence on energy efficiency [8]. Juarez and Brown analyzed the effect of strong turbulence on the Strehl ratio (SR) of a free-space optical communication system [9].

In most of the aforementioned studies, SR was used as a criterion for evaluating the effect of atmospheric turbulence on the BER of a free-space laser communication system. When the SR method is utilized, the effect of the area of the laser-receiving end face is disregarded. However, the area of the laser-receiving end face will actually affect the receiving energy of the laser. The power-in-the-bucket (PIB) is defined as all the power within a circular region in the cross section of laser beam, and the radius of the circular region is defined as the bucket radius [10]. As it is related to the area of receiving end face, PIB is more suitable to calculate the receiving energy. Some researchers have tried to use PIB to calculate receiving energy [11]. But no concrete formulas are given. Ji *et al.* studied the degradation of PIB for the laser beam propagating through the turbulence and obtained a specific equation [12]. Nevertheless, they have no consideration of the receiving optical system. Therefore, the effects of both the atmospheric turbulence and receiving system on the receiving energy will be considered, and a concrete formula will be given. This work is helpful for the accurate evaluation of the communication quality of free-space laser communication and the design of the communication receiving systems.

2. THEORY

A. Effect of Atmospheric Turbulence on PIB

A simple model (Fig. 1) is established to analyze the effect of atmospheric turbulence on PIB. The laser with an initial phase of ϕ_0 propagates through the atmospheric turbulence, and its

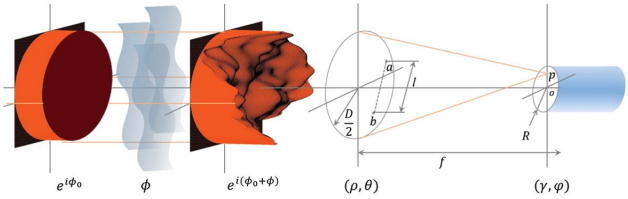

Fig. 1. Schematic of PIB.

phase is distorted by the turbulence with phase ϕ. The diameter of the entrance pupil is D, the focal length of the optical system is f, and the radius of the receiving end face is R. The entrance pupil and focal planes are expressed with the polar coordinates (ρ, θ) and (γ, φ), respectively. Thus, the received energy can be expressed with PIB, i.e.,

$$\mathrm{PIB} = \int_0^R \int_0^{2\pi} I[p(\gamma,\varphi)]\gamma \mathrm{d}\gamma \mathrm{d}\varphi. \tag{1}$$

The Huygens–Fresnel principle indicates that the light intensity of point p may be described by [12]

$$\begin{aligned} I(p) &= U[p(\gamma,\varphi)] \cdot U^*[p(\gamma,\varphi)] \\ &= \left(\frac{AD^2}{4\lambda f^2}\right)^2 \times \left| \int_0^1 \int_0^{2\pi} \exp\left[i\phi(\rho,\theta) \right.\right. \\ &\quad \left.\left. -\frac{iD}{2f}\rho\gamma\cos(\theta-\varphi)\right]\rho \mathrm{d}\rho \mathrm{d}\theta \right|^2, \end{aligned} \tag{2}$$

where the initial phase ϕ_0 is disregarded to simplify the discussion; A is the amplitude of the incident optical field; λ is the wavelength of the laser; and U is the complex amplitude, which can be represented as

$$\begin{aligned} U(p) &= -\frac{iAD^2}{4\lambda f^2} \times \int_0^1 \int_0^{2\pi} \\ &\quad \times \exp\left\{ i\left[\phi(\rho,\theta) - \frac{D}{2f}\rho\gamma\cos(\theta-\varphi)\right]\right\}\rho \mathrm{d}\rho \mathrm{d}\theta. \end{aligned} \tag{3}$$

Theoretically, PIB may be calculated by substituting Eq. (2) into Eq. (1). However, the formula is complicated to analyze the effect of turbulence on PIB. The formula for PIB is then simplified, as shown in the Appendix A. The simplified PIB may be expressed as

$$\mathrm{PIB} = \zeta \int_S \int_S \exp[i\phi(\boldsymbol{\rho}_1)]\exp^*[i\phi(\boldsymbol{\rho}_2)]\frac{2RJ_1(\pi Rl)}{l} d\boldsymbol{\rho}_1 d\boldsymbol{\rho}_2, \tag{4}$$

where $\boldsymbol{\rho}_1$ and $\boldsymbol{\rho}_2$ are the coordinates of two arbitrary points on the pupil plane, l is the distance between $\boldsymbol{\rho}_1$ and $\boldsymbol{\rho}_2$, J_1 is the first-order Bessel function, and ζ is defined as

$$\zeta = \left(\frac{AD^2}{4\lambda f^2}\right)^2. \tag{5}$$

Equation (4) can be rewritten as

$$\begin{aligned} \mathrm{PIB} &= \zeta \int_0^2 \mathrm{d}l \int_S \mathrm{d}\boldsymbol{\rho}\left\{ \exp[i\phi(\boldsymbol{\rho})]\exp^*[i\phi(\boldsymbol{\rho}+l)]\frac{2RJ_1(\pi Rl)}{l}\right\} \\ &= \zeta \int_0^2 \frac{2RJ_1(\pi Rl)}{l}\mathrm{d}l \int_S \exp[i\phi(\boldsymbol{\rho})]\exp^*[i\phi(\boldsymbol{\rho}+l)]\mathrm{d}\boldsymbol{\rho}. \end{aligned} \tag{6}$$

As light goes through the atmospheric turbulence, its phase ϕ will be distorted, and PIB will be affected according to Eq. (6). The atmospheric turbulence is random, and thus, the statistical average of PIB may be written as

$$\begin{aligned} \langle \mathrm{PIB} \rangle &= \zeta \int_0^2 \left\langle \int_S \exp[i\phi(\boldsymbol{\rho})]\exp^*[i\phi(\boldsymbol{\rho}+l)]\mathrm{d}\boldsymbol{\rho} \right\rangle \\ &\quad \times \frac{2RJ_1(\pi Rl)}{l}\mathrm{d}l. \end{aligned} \tag{7}$$

In Eq. (7), the statistical average part can be rewritten as

$$\begin{aligned} &\left\langle \int_S \exp[i\phi(\boldsymbol{\rho})]\exp^*[i\phi(\boldsymbol{\rho}+l)]\mathrm{d}\boldsymbol{\rho} \right\rangle \\ &= \int_S \langle \exp[i\phi(\boldsymbol{\rho})]\exp^*[i\phi(\boldsymbol{\rho}+l)]\rangle \mathrm{d}\boldsymbol{\rho} \\ &= \int_S \exp[i\langle \phi(\boldsymbol{\rho}) - \phi(\boldsymbol{\rho}+l)\rangle]\mathrm{d}\boldsymbol{\rho} \\ &= \int_S \cos(\langle \Delta\phi_l \rangle)\mathrm{d}\boldsymbol{\rho} \\ &= \pi^2 f(l|S)\mathrm{d}l \cdot \int_{-\infty}^{\infty} \cos(\Phi) f(\Phi)\mathrm{d}\Phi, \end{aligned} \tag{8}$$

where $\Phi = \phi(\boldsymbol{\rho}) - \phi(\boldsymbol{\rho}+l)$; $f(l|S)$ is the distribution density of l over area S; and $f(\Phi)$ is the distribution density of Φ, which follows normal distribution with an expectation of zero. Thus, $f(\Phi)$ may be expressed as

$$f(\Phi) = \frac{1}{\sqrt{2\pi\langle\Phi^2\rangle}} \exp\left(-\frac{\Phi^2}{2\langle\Phi^2\rangle}\right). \tag{9}$$

The Kolmogorov model of atmospheric turbulence indicates that the variance of Φ is given by [13]

$$\langle\Phi^2\rangle = \langle[\phi(\boldsymbol{\rho}) - \phi(\boldsymbol{\rho}+l)]^2\rangle = 6.88\left(\frac{l}{r_0}\right)^{\frac{5}{3}}, \tag{10}$$

where r_0 is the atmospheric coherence length. Then, $f(\Phi)$ may be rewritten as

$$f(\Phi) = \frac{\left(\frac{r_0}{l}\right)^{\frac{5}{6}}}{\sqrt{13.76\pi}} \exp\left[-\frac{\Phi^2}{13.76}\left(\frac{r_0}{l}\right)^{\frac{5}{3}}\right]. \tag{11}$$

$f(l|S)$ should also be described in detail to obtain the exact and calculable expressions of $\langle \mathrm{PIB} \rangle$. A circular aperture without obstruction is selected as an example to deduce the expression for $f(l|S)$. As shown in Fig. 2(a), the pupil aperture is assumed as a unit circle with a diameter of 2. Point A belongs to the annulus with a radius of r and a width of dr. Thus, the distribution density of point A can be obtained from the ratio of the annulus area to the unit circle area, i.e.,

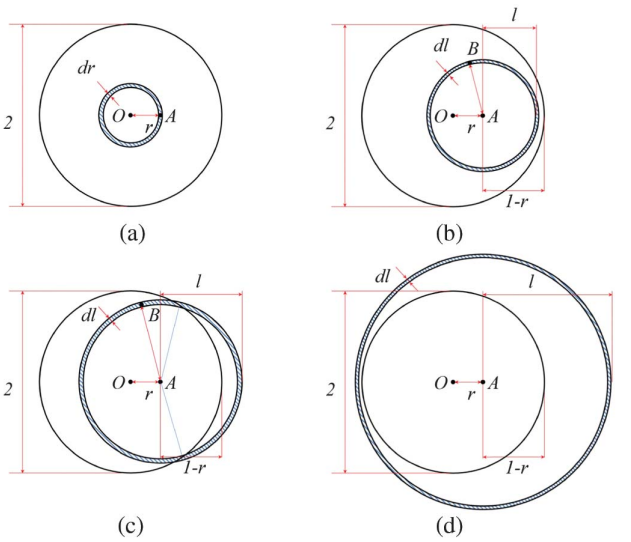

Fig. 2. Diagram of $f(l|S)$ in a unit circle: (a) probability of point a with a distance of r from the center, (b) $l \le 1-r$, (c) $1-r<l<1+r$, and (d) $l>1+r$.

$$f(r|S)=f(A)=\frac{2\pi r}{\pi}dr=2rdr. \tag{12}$$

Point B has a distance l from A, and it should be in the annulus that is centered at A with a radius of l and a width of dl, as shown in Figs. 2(b) and 2(c). The distance l has three conditions: (1) $l<1-r$, as shown in Fig. 2(b); (2) $1-r<l\le 1+r$, as shown in Fig. 2(c), which represents the annulus area within the unit circle area; and (3) $l>1+r$, which is the part of the annulus beyond the circle area, as shown in Fig. 2(d). Thus, the distribution density of point B may be described as

$$f(l|r)=f(B|A)=\begin{cases}2ldl, & l\le 1-r\\ \frac{2l}{\pi}\arccos\left(\frac{r^2+l^2-1}{2rl}\right)dl, & 1-r<l\le 1+r\\ 0, & l>1+r\end{cases}. \tag{13}$$

The distribution density $f(l|S)$ can be written as the product of Eqs. (12) and (13) as follows:

$$f(l|S)=\int_0^1 f(l|r)f(r|S)\mathrm{d}r \approx (0.15l^4-0.275l^3-l^2+2l)\mathrm{d}l. \tag{14}$$

The average PIB can be acquired as follows by combining Eqs. (7), (8), (11), and (14):

$$\langle \mathrm{PIB}\rangle=\pi^2\zeta\int_0^2\left[2l(1-l)^2+\int_{1-l}^{l}\frac{4rl}{\pi}\arccos\left(\frac{r^2+l^2-1}{2rl}\right)dr\right]\times\left\{\int_{-\infty}^{\infty}\cos(\Phi)\frac{\left(\frac{r_0}{l}\right)^{\frac{5}{6}}}{\sqrt{13.76\pi}}\exp\left[-\frac{\Phi^2}{13.76}\left(\frac{r_0}{l}\right)^{\frac{5}{3}}\right]\mathrm{d}\Phi\right\}\times\frac{2RJ_1(\pi Rl)}{l}\mathrm{d}l. \tag{15}$$

The average PIB is related to r_0 and the aperture of the receiving end face R. Consequently, the PIB can be calculated accurately from the known r_0 and R. In free-space laser communication, the normalized PIB is always used and may be written as

$$\langle \mathrm{PIB}_{\mathrm{norm}}\rangle=\frac{\langle \mathrm{PIB}\rangle}{\mathrm{Power}_{\mathrm{No\ turbulence}}}=\frac{\langle \mathrm{PIB}\rangle}{A^2\left(\frac{\pi D^2}{4}\right)}, \tag{16}$$

where $\mathrm{Power}_{\mathrm{No\ turbulence}}$ represents the total receiving power without the turbulence effect.

The turbulence strength D/r_0 is changed from 0.5 to 20, and the aperture of the receiving end face R/R_A is altered from 0.08 to 5 to compute the effects of r_0 and R on PIB. R_A is the ideal radius of the Airy disk, and it is equal to $1.22f\lambda/D$. The change in the normalized PIB is computed as shown in Fig. 3. The color bar represents the value of the normalized PIB. The PIB contours are also shown in Fig. 3, with an interval of 0.1. The PIB is improved with increases in r_0 and R. Along with a certain contour, the expected PIB can be designed with different combinations of parameters for free-space laser communication systems. Three typical contours are fitted as follows:

$$\begin{aligned}\langle \mathrm{PIB}_{\mathrm{norm}}\rangle=90\%: &\quad \frac{RD}{f\lambda}=0.8\frac{D}{r_0}+1.8\\ \langle \mathrm{PIB}_{\mathrm{norm}}\rangle=80\%: &\quad \frac{RD}{f\lambda}=0.7\frac{D}{r_0}+0.8\\ \langle \mathrm{PIB}_{\mathrm{norm}}\rangle=50\%: &\quad \frac{RD}{f\lambda}=0.5\frac{D}{r_0}+0.4.\end{aligned} \tag{17}$$

The SR is also calculated using the formula to compare with the SR method [14], i.e.,

$$\mathrm{SR}\approx\left[1+\left(\frac{D}{r_0}\right)^{\frac{5}{3}}\right]^{-\frac{6}{5}}. \tag{18}$$

Figure 4(a) shows the normalized receiving energy as a function of D/r_0 for the PIB and SR methods under the condition of $R=1.22f\lambda/D$. Although the change tendency is similar, the computed normalized receiving energy of the PIB method is higher than that of the SR method. For $D/r_0=4$, the relation between the normalized receiving energy and R/R_A is shown in Fig. 4(b) for the PIB and SR methods. The normalized receiving energy increases with an increase in the aperture of the receiving end face for the PIB method. For the SR method, however, the normalized receiving energy is a constant. The energy distribution is distorted, and the area is enlarged due to the effect of turbulence. An increase in

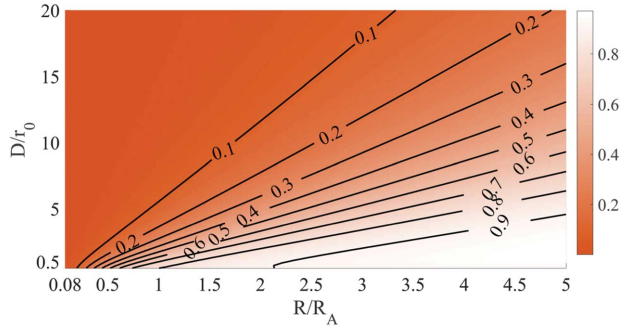

Fig. 3. PIB as a function of atmospheric coherent length and the aperture of the receiving end face.

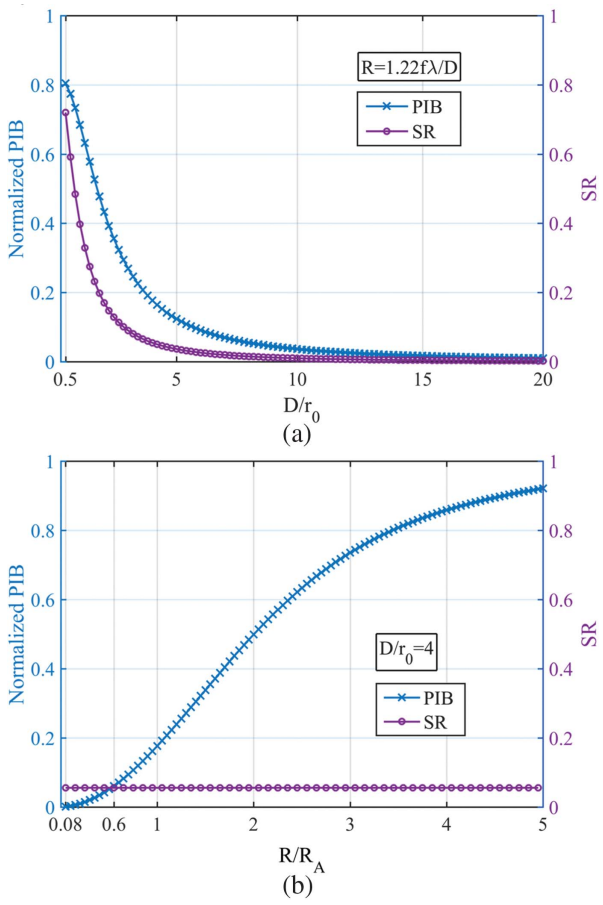

Fig. 4. Calculated results of the PIB and SR methods: (a) changed with D/r_0 and (b) changed with R/R_A.

the receiving aperture will also increase the received energy. Therefore, the PIB method may compute the received energy more accurately than the SR method. Two curves exhibit a crossover with $R/R_A = 0.6$. When R is 0.6 times the Airy disk, the calculated results of the PIB and SR methods are the same under the condition of $D/r_0 = 4$. When the receiving aperture deviates from this point, the evaluation error will be increased for the SR method. That is, the SR method is effective only at this point to evaluate the receiving energy of free-space laser communication systems.

B. Relation Between PIB and BER

For free-space laser communication, the turbulence effect on the BER of the communication system is expected to be known. Therefore, BER, as a function of PIB, should be achieved to evaluate the turbulence effect. The "zero" bit and "one" bit are assumed to be uncorrelated, and the BER of the homenergic binary code can be expressed as [15]

$$\mathrm{BER} = \frac{1}{2}\,\mathrm{erfc}\left(\sqrt{\frac{\mathrm{PIB}}{2n_0}}\right), \tag{19}$$

where n_0 is the energy of noise; SNR is the signal-to-noise ratio; and erfc is the complementary error function, which can be written as

$$\mathrm{erfc}(x) = 1 - \frac{2}{\sqrt{\pi}}\int_0^x \exp(-z^2)\mathrm{d}z. \tag{20}$$

The BER of the communication system can be calculated with the known PIB and n_0 according to Eq. (19). The BER of fiber optical communication is approximately 10^{-9}, and $\mathrm{PIB}/(2n_0)$ is approximately 36 according to Eqs. (19) and (20). Thus, when using the fiber to receive the laser, the BER as a function of PIB may be written as

$$\langle \mathrm{BER} \rangle = \frac{1}{2}\,\mathrm{erfc}\left(\sqrt{18\langle \mathrm{PIB}_{\mathrm{norm}} \rangle}\right). \tag{21}$$

BER can be computed according to Eq. (21) by using the data in Fig. 4, and the results are presented in Fig. 5. Figure 5(a) shows the BER as a function of turbulence intensity. Communication quality is decreased drastically with an increase in turbulence intensity. Therefore, the atmospheric turbulence seriously affects free-space laser communication. The effect of the aperture of the receiving end face on BER is shown in Fig. 5(b). BER is reduced with an increase in the receiving area. For the SR method, however, the calculated BER is a constant with a change in the receiving area. Consequently, the PIB method is more effective for evaluating the communication quality of free-space laser communication.

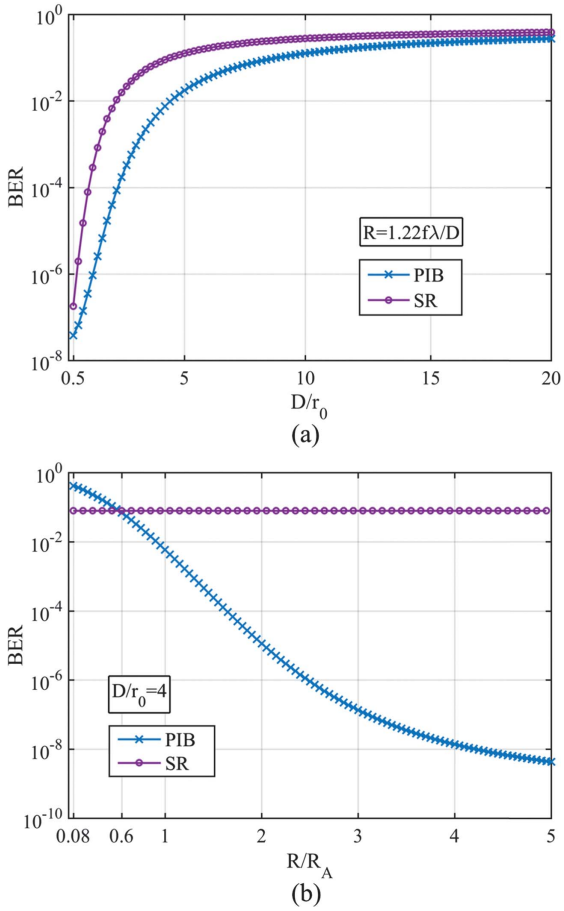

Fig. 5. Calculated BER using the PIB and SR methods: (a) changed with D/r_0 and (b) changed with R/R_A.

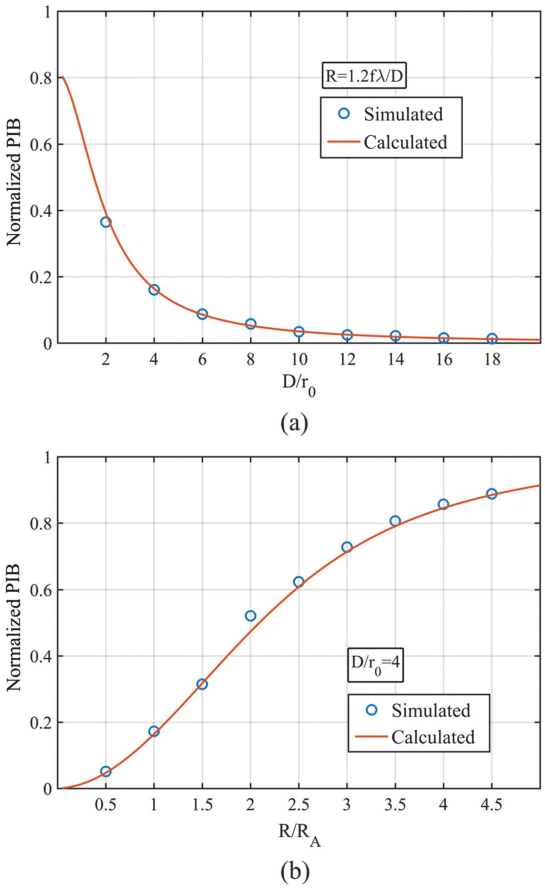

Fig. 6. Simulated and calculated PIBs versus (a) D/r_0 and (b) R/R_A.

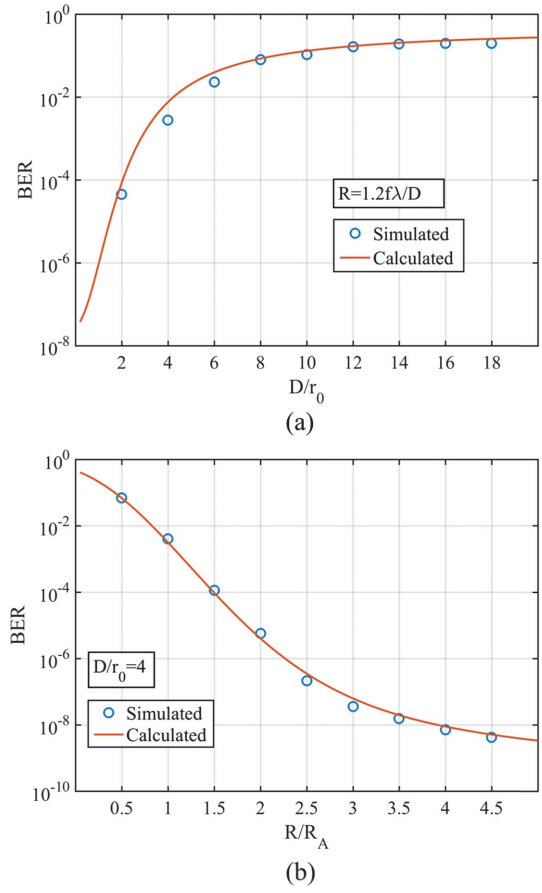

Fig. 7. Simulated and calculated BERs versus (a) D/r_0 and (b) R/R_A.

C. Verification with Simulated Turbulence

The atmospheric turbulence is simulated using Noll's method [16] to validate the PIB equation. The optical setup model is used, as shown in Fig. 1. Distorted wavefronts are first produced using Noll's method. The turbulence effect on the optical field distribution of the focal plane may then be calculated via fast Fourier transform (FFT). Thus, the simulated PIB can be computed by

$$\mathrm{PIB}_{\mathrm{simulated}} = \int \{\mathrm{FFT}[\exp(i\phi_{\mathrm{simulated}})] \cdot W(R)\}, \qquad (22)$$

where $W(R)$ is the aperture function, which indicates that only the light intensity within the receiving area is calculated. The simulated PIB can be calculated from assured r_0 and R. It can also be computed using Eq. (15). Thus, the difference between the simulated and theoretical results may be obtained, and the validation of Eq. (15) can be evaluated. The first 231 modes of Zernike polynomials are used to simulate the atmospheric turbulence. Then, 100 atmospheric turbulence wavefronts are utilized to acquire the statistical average of PIB.

The parameters used in Fig. 4 are selected to perform the simulation to confirm the validation of Eq. (15), and the simulated results are shown in Fig. 6. The circle and the real line represent the simulated and calculated results, respectively. The simulated results are close to the calculated results. Consequently, the deduced theoretical equations can be considered valid for the calculation of PIB. The BER of the communication system is simulated as well, and the results are shown in Fig. 7. It indicates that the BERs of simulated and calculated are consistent. The results prove that the PIB method may be used to evaluate the communication quality.

3. VALIDATION EXPERIMENT

An experiment is performed to validate the PIB formula, and the optical layout is shown in Fig. 8. A laser with a wavelength of 808 nm is outputted with a single-mode fiber and collimated by a collimating lens. The collimated light goes through an atmospheric turbulence simulator and is then split into two beams with a beam splitter (BS). The transmitted light is focused on the pinhole and then measured with an optical power meter. The reflected beam is reflected again by a mirror and then focused on a CCD camera. The turbulence simulator (Lexitek, Inc.) is utilized to produce the atmospheric turbulence with aperture of 100 mm. Its operating principle is based on the frozen turbulence hypothesis. The r_0 may be changed by adjusting the size of the beam passing through the simulator, and the Greenwood frequency is changed by tuning the rotation rates.

We first validate the relation between the average PIB and D/r_0. As the r_0 of each turbulence simulator is constant and

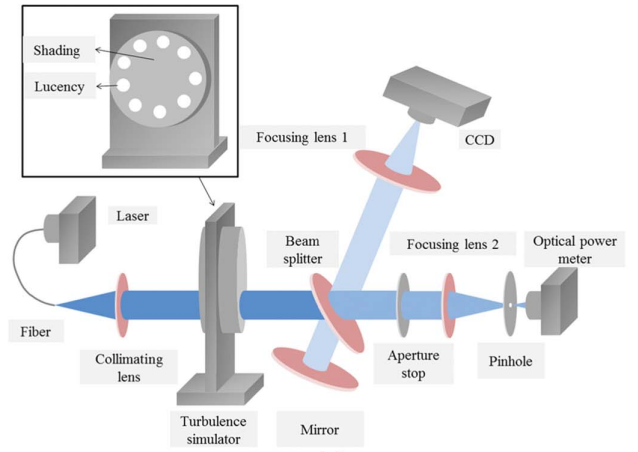

Fig. 8. Optical layout for evaluation: (a) design and (b) experimental setup.

the beam size cannot be changed for a certain optical system, different simulators have to be used to change the r_0. In the experiment, three simulators are selected with $D/r_0 = 2.1$, 4, and 6.9, which represent weak, moderate, and strong turbulence, respectively. The 808 nm laser is emitted and propagates through the turbulence simulator with a beam size of 10 mm. A pinhole is used as the receiving end face with a diameter of 15 μm. As shown in Fig. 8(a), nine sub-apertures are chosen to obtain the statistical average of the atmospheric turbulence. The PIB is measured by an optical power meter, which is followed by the pinhole. The measured and calculated results are shown in Fig. 9 by changing the D/r_0. The dot represents the measured result, and each dot is acquired with the average of nine measured values. It can be seen that the measured results

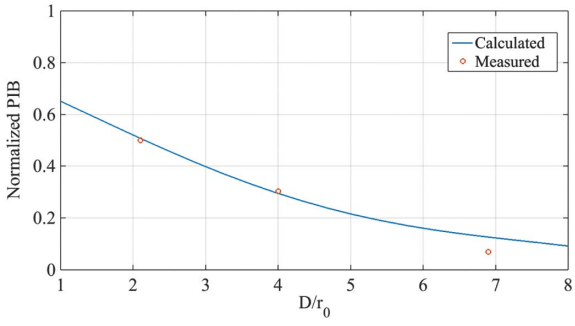

Fig. 9. Measured and calculated PIB versus D/r_0.

accord with the theoretical curve very well. The root mean square (RMS) value of the deviation between the measured and calculated results is 0.03. Therefore, it illustrates that the PIB as a function of D/r_0 is valid.

The effect of the aperture of the receiving end face is also validated by changing the diameter of the pinhole. In the experiment, four pinholes are selected with diameters of 15, 25, 50, and 100 μm. The diameter of the Airy disk without distortion is 25 μm, which is produced by adjusting the aperture stop. Then we put a mask with nine sub-apertures on the simulator of $D/r_0 = 4$, as shown in Fig. 8. Before the turbulence simulator is placed into the optical layout, nine sub-apertures are measured by a Shack–Hartmann wavefront sensor (S–H WFS) to get the specific aberration Zernike coefficients. In the experiment, different sub-apertures are used in turn, and the PIBs are measured accordingly using an optical power meter. For a normal laser communication system, the tip-tilt will be corrected by the acquiring-pointing-tracking (APT) system. Therefore, the effect of the tip-tilt of the turbulence should be eliminated in the experiment. Accordingly, a CCD camera is used to remember the reference position, and the concrete process is as follows. First, for the optical layout without the turbulence simulator, the 808 nm laser is outputted, and the pinhole is moved to the position where the receiving energy is maximal. Afterward, the optical power meter is removed, and another light source is placed behind the pinhole. Thus, two light points are imaged simultaneously at the CCD camera. The two light points can overlap completely by adjusting the BS. At this time, the light point of the CCD camera is conjugated to the pinhole. The tip-tilt will be produced when the turbulence simulator is placed into the optical layout, and the light point of the 808 nm laser will be moved. Two light points will again appear in the CCD camera. The pinhole is moved to assure that the two light points are superposed once more to eliminate the effect of the tip-tilt. Consequently, the laser will be focused on the pinhole, and the effect of the tip-tilt is eliminated. The CCD camera is also used to replace the pinhole. Before replacing the pinhole, the laser is turned off and the pinhole is illuminated by the light source behind it. A light point will be imaged at the CCD camera, and the position is recorded. At this time, the pinhole is replaced, and the new pinhole is moved until the light point is moved to the recorded position. The RMS error of the nine sub-apertures measured with S–H WFS is shown in Table 1.

Table 1. RMS of Each Sub-aperture Measured with S–H WFS

Number of Sub-aperture	RMS(λ)
1	0.2151
2	0.1318
3	0.2263
4	0.1426
5	0.2923
6	0.1642
7	0.1069
8	0.1602
9	0.1282

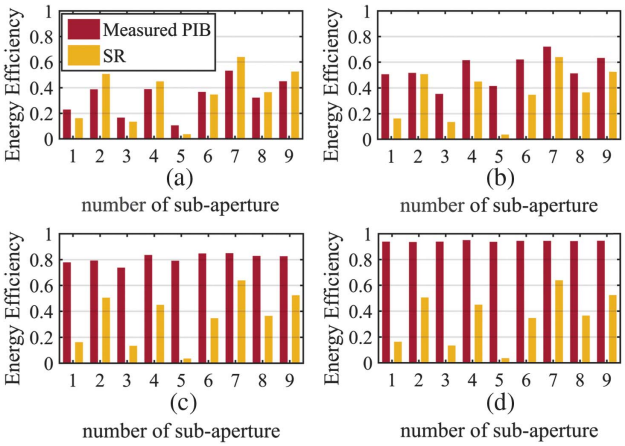

Fig. 10. Measured PIB and SR with different pinholes: (a) 15 μm, (b) 25 μm, (c) 50 μm, and (d) 100 μm.

For each pinhole, the PIB is measured in turn with nine sub-apertures, and the PIBs of different pinholes are determined. To compare with the SR method, the SR is computed by [17]

$$\mathrm{SR} \approx \exp(-\Delta\phi^2), \tag{23}$$

where $\Delta\varphi$ is the RMS error of the wavefront distortion, and it can be calculated with the measured wavefronts. The calculated SR and measured PIB for different pinholes are shown in Fig. 10. For each pinhole, nine positions of the turbulence simulator are used to acquire the statistical average.

PIB is also calculated with $D/r_0 = 4$ to validate theoretical Eq. (15). The tip-tilt of the turbulence is removed in the experiment and in the theoretical calculation. The calculated and measured results are shown in Fig. 11. The measured results are the statistical average values acquired with the data in Fig. 8. The theoretical curve is close to the measured data. The measured PIBs are used as the ideal value to evaluate the deviation magnitude, and the deviations are computed for the PIB and SR methods, as shown in Fig. 12. The deviation in the calculated PIB is minimal, and the maximum deviation is less than 14%. By contrast, the deviation in the SR method changes drastically, and the largest deviation is over 60%. Nevertheless, the deviation in the SR method at $R/R_A = 0.6$ is 15%, and the SR method is effective at this point. Therefore, the experimental results indicate that the theoretical equations are valid, and

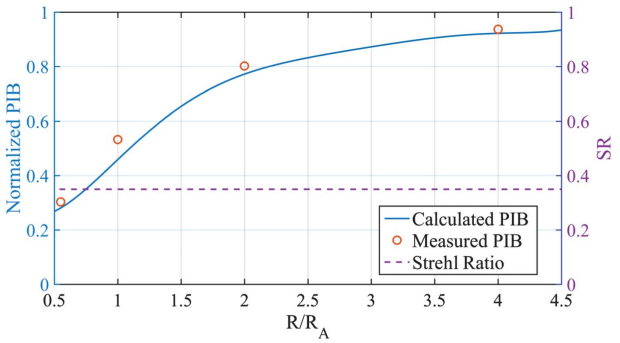

Fig. 11. Comparison between the measured and calculated results of PIB and SR.

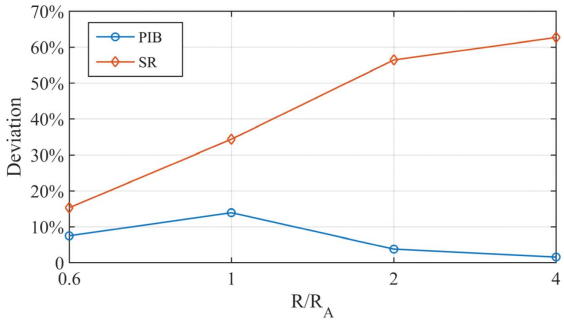

Fig. 12. Deviation of the calculated PIB and SR results from the ideal value.

the receiving energy of a free-space laser communication system can be calculated using the PIB method.

4. CONCLUSIONS

The PIB method is established to accurately evaluate the effect of turbulence on the receiving energy of a free-space laser communication system. A theoretical deduction is performed to acquire the PIB formula with the turbulence effect. As an example, the BER expression is provided for the fiber receiving system. The calculated results show that although the change tendency is similar, the computed receiving energy of the PIB is larger than that of the SR at different turbulence strengths. For $D/r_0 = 4$, the normalized receiving energy is increased with an increase in the aperture of the receiving end face for the PIB method. By contrast, the normalized receiving energy is a constant with an increase in the receiving aperture for the SR method. Two curves exhibit a crossover with $R/R_A = 0.6$. They illustrate that the PIB method can accurately describe the receiving energy, but the SR method is effective only at one point. The computed BER results can derive similar conclusions.

A simulation validation is performed to verify the theoretical equation. The distorted wavefronts are produced using Noll's method, and FFT is used to analyze the distribution of light intensity. The simulated results show that the simulated points fit perfectly with the theoretical curve. An experiment is also performed to validate the theoretical equation. The results show that the calculated results become close to the measured results of the PIB method with an increase in the receiving aperture and the D/r_0. To different receiving apertures, the maximum deviation in the PIB method is less than 14%, whereas that in the SR method is over 60%.

All the results show that, compared with the SR method, the PIB method is more suitable for calculating the receiving energy of a free-space laser communication system. This work is helpful for the design and evaluation of the communication quality of free-space laser communication systems.

APPENDIX A: SIMPLIFICATION OF PIB FORMULA

For simplification, the double integral Eq. (3) is transformed into a single integral form as follows:

$$
\begin{aligned}
&U[p(\gamma,\varphi)]\\
&=-\frac{iAD^2}{4\lambda f^2}\int_0^1\int_0^{2\pi}\exp\left\{i\left[\phi(\rho_1,\phi_1)\right.\right.\\
&\left.\left.-\frac{D}{2f}\rho_1\gamma\cos(\theta_1-\varphi)\right]\right\}\rho_1\mathrm{d}\rho_1\mathrm{d}\theta_1\\
&=-\frac{iAD^2}{4\lambda f^2}\int_S\exp\left\{i\left[\phi(\rho_1,\phi_1)-\frac{D}{2f}\rho_1\gamma\cos(\theta_1-\varphi)\right]\right\}\mathrm{d}\boldsymbol{\rho}_1,
\end{aligned}
\tag{A1}
$$

$$
\begin{aligned}
&U^*[p(\gamma,\varphi)]\\
&=-\frac{iAD^2}{4\lambda f^2}\int_0^1\int_0^{2\pi}\exp\left\{i\left[-\phi(\rho_2,\phi_2)\right.\right.\\
&\left.\left.-\frac{D}{2f}\rho_2\gamma\cos(\theta_2-\varphi)\right]\right\}\rho_2\mathrm{d}\rho_2\mathrm{d}\theta_2\\
&=-\frac{iAD^2}{4\lambda f^2}\int_S\exp\left\{i\left[-\phi(\rho_2,\phi_2)+\frac{D}{2f}\rho_2\gamma\cos(\theta_2-\varphi)\right]\right\}\mathrm{d}\boldsymbol{\rho}_2,
\end{aligned}
\tag{A2}
$$

where S denotes the area of the unit circle; $\boldsymbol{\rho}(\rho,\theta)$ represents the coordinates of the point in the pupil plane; and $\boldsymbol{\rho_1}(\rho_1,\theta_1)$ and $\boldsymbol{\rho_2}(\rho_2,\theta_2)$ are the coordinates of points a and b, respectively. Then, Eq. (2) may be rewritten as

$$
\begin{aligned}
&I[p(\gamma,\varphi)]\\
&=U[p(\gamma,\varphi)]\cdot U^*[p(\gamma,\varphi)]\\
&=\zeta\int_S\exp\left\{i\left[\phi(\rho_1,\phi_1)-\frac{D}{2f}\rho_1\gamma\cos(\theta_1-\varphi)\right]\right\}d\boldsymbol{\rho}_1\\
&\times\int_S\exp\left\{i\left[-\phi(\rho_2,\phi_2)+\frac{D}{2f}\rho_2\gamma\cos(\theta_2-\varphi)\right]\right\}\mathrm{d}\boldsymbol{\rho}_2\\
&=\zeta\int_S\int_S\exp[i(\phi_1-\phi_2)]\cdot\exp\left\{i\frac{D}{2f}[\rho_2\gamma\cos(\theta_2-\varphi)\right.\\
&\left.-\rho_1\gamma\cos(\theta_1-\varphi)]\right\}d\boldsymbol{\rho}_1d\boldsymbol{\rho}_2\\
&=\zeta\int_S\int_S\exp[i(\phi_1-\phi_2)]\exp(i\pi rl_x\cos\varphi)\\
&\times\exp(i\pi rl_y\sin\varphi)d\boldsymbol{\rho}_1d\boldsymbol{\rho}_2,
\end{aligned}
\tag{A3}
$$

where

$$l_x=\rho_2\cos\theta_2-\rho_1\cos\theta_1, \tag{A4}$$

$$l_y=\rho_2\sin\theta_2-\rho_1\sin\theta_1, \tag{A5}$$

$$r=\frac{D}{f\lambda}\gamma. \tag{A6}$$

lx and ly are the distances between points a and b in the x and y directions, respectively. The e-index function of Eq. (A3) can be transformed using the Jacobi–Anger identity [18]:

$$e^{iz\cos\psi}=\sum_{t=-\infty}^{\infty}i^tJ_t(z)e^{it\psi}, \tag{A7}$$

$$e^{iz\sin\psi}=\sum_{t=-\infty}^{\infty}J_t(z)e^{it\psi}, \tag{A8}$$

where $Jt(z)$ is the t-order Bessel function. When Eqs. (A7) and (A8) are substituted into Eq. (A3), we may derive

$$
\begin{aligned}
I(p)=\zeta&\int_S\int_S\exp[i(\phi_1-\phi_2)]\\
&\times\left[\sum_{m=-\infty}^{\infty}\sum_{n=-\infty}^{\infty}i^mJ_m(\pi l_xr)J_n(\pi l_yr)e^{im\varphi}e^{in\varphi}\right]\mathrm{d}\boldsymbol{\rho_1}\mathrm{d}\boldsymbol{\rho_2}.
\end{aligned}
\tag{A9}
$$

When Eq. (A9) is substituted into Eq. (1), PIB can be described as

$$
\begin{aligned}
\mathrm{PIB}=\zeta&\int_S\int_S\exp[i(\phi_1-\phi_2)]\\
&\times\left[\int_0^R\sum_{m=-\infty}^{\infty}\sum_{n=-\infty}^{\infty}i^mJ_m(\pi l_xr)J_n(\pi l_yr)r\mathrm{d}r\int_0^{2\pi}e^{im\varphi}e^{in\varphi}\mathrm{d}\varphi\right]\\
&\times\mathrm{d}\boldsymbol{\rho_1}\mathrm{d}\boldsymbol{\rho_2}.
\end{aligned}
\tag{A10}
$$

The integral $\int_0^{2\pi}e^{im\varphi}e^{in\varphi}\mathrm{d}\varphi$ is equal to zero, except for $m=-n$. Thus, Eq. (A10) may be simplified as

$$
\begin{aligned}
\mathrm{PIB}=\zeta&\int_S\int_S\mathrm{d}\boldsymbol{\rho_1}\mathrm{d}\boldsymbol{\rho_2}\exp[i(\phi_1-\phi_2)]\\
&\times\int_0^R r\mathrm{d}r\left[2\pi\sum_{m=-\infty}^{\infty}i^mJ_m(\pi l_xr)J_{-m}(\pi l_yr)\right].
\end{aligned}
\tag{A11}
$$

The Bessel function in the Sturm–Liouville style is [19]

$$\frac{d}{dr}\left(r\frac{dJ(r)}{dr}\right)+\left(qr-\frac{\upsilon^2}{r}\right)J(r)=0, \tag{A12}$$

where q is the eigenvalue. $J(\pi l_xr)$ and $J(\pi l_yr)$ can be set as the eigenfunctions with eigenvalues of πl_x and πl_y. Two equations may be obtained [20], namely,

$$
\begin{aligned}
&J_m(\pi l_xr)\frac{d}{dr}\left[r\frac{d}{dr}J_m(\pi l_yr)\right]\\
&+\left(\pi^2l_y^2r-\frac{\upsilon^2}{r}\right)J_m(\pi l_xr)J_m(\pi l_yr)=0,
\end{aligned}
\tag{A13}
$$

$$
\begin{aligned}
&J_m(\pi l_yr)\frac{d}{dr}\left[r\frac{d}{dr}J_m(\pi l_xr)\right]\\
&+\left(\pi^2l_x^2r-\frac{\upsilon^2}{r}\right)J_m(\pi l_xr)J_m(\pi l_yr)=0.
\end{aligned}
\tag{A14}
$$

The recursion formula of the Bessel function is

$$xJ'_m(x)=xJ_{m-1}(x)-mJ_m(x), \tag{A15}$$

where J'_m is the first derivative of Jm. When Eq. (A14) is subtracted from Eq. (A13) and then 0 to R is integrated into the recursion formula, we can obtain

$$\int_0^R J_m(\pi l_x r) J_m(\pi l_y r) r \mathrm{d}r = \frac{1}{\pi(l_x^2 - l_y^2)} [l_y R J_{m-1}(\pi l_y R) J_m(\pi l_x R) - l_x R J_{m-1}(\pi l_x R) J_m(\pi l_y R)]. \quad \textbf{(A16)}$$

Thus, the latter part of Eq. (A11) may be rewritten as

$$\int_0^R r \mathrm{d}r \left[2\pi \sum_{m=-\infty}^{\infty} i^m J_m(\pi l_x r) J_{-m}(\pi l_y r) \right] = \frac{2R}{l_x^2 - l_y^2} \left[l_y \sum_{m=-\infty}^{\infty} (-i)^m J_m(\pi l_x R) J_{m-1}(\pi l_y R) - l_x \sum_{m=-\infty}^{\infty} (-i)^m J_m(\pi l_y R) J_{m-1}(\pi l_x R) \right]. \quad \textbf{(A17)}$$

The Graf's generalization of Neumann's formula is as follows [21]:

$$J_\upsilon(\varpi) \left(\frac{x - y e^{-i\psi}}{x - y e^{i\psi}} \right)^{\frac{1}{2}\upsilon} = \sum_{m=-\infty}^{\infty} J_{m+\upsilon}(x) J_m(y) e^{im\psi}, \quad \textbf{(A18)}$$

where

$$\varpi = \sqrt{x^2 + y^2 - 2xy \cos \psi}. \quad \textbf{(A19)}$$

Under the conditions of $\upsilon = -1$ and $\psi = -\pi/2$, we can acquire

$$\sum_{m=-\infty}^{\infty} (-i)^m J_m(\pi l_x R) J_{m-1}(\pi l_y R) = \mathrm{sgn}(l_x l_y) \mathrm{sgn}(l_x) J_{-1}\left(\pi R \sqrt{l_x^2 + l_y^2} \right) \left(\frac{l_y - i l_x}{l_y + i l_x} \right)^{-\frac{1}{2}}, \quad \textbf{(A20)}$$

$$\sum_{m=-\infty}^{\infty} (-i)^m J_m(\pi l_y R) J_{m-1}(\pi l_x R) = \mathrm{sgn}(l_x l_y) \mathrm{sgn}(l_y) J_{-1}\left(\pi R \sqrt{l_x^2 + l_y^2} \right) \left(\frac{l_x - i l_y}{l_x + i l_y} \right)^{-\frac{1}{2}}. \quad \textbf{(A21)}$$

When Eqs. (A20) and (A21) are substituted into Eq. (A17), the latter part of Eq. (A11) may be described as

$$\int_0^R r \mathrm{d}r \left[2\pi \sum_{m=-\infty}^{\infty} i^m J_m(\pi l_x r) J_{-m}(\pi l_y r) \right] = \frac{2R J_1\left(\pi R \sqrt{l_x^2 + l_y^2} \right)}{\sqrt{l_x^2 + l_y^2}}, \quad \textbf{(A22)}$$

where $\sqrt{l_x^2 + l_y^2} = l$ and is the distance between the arbitrary two points on the pupil plane.

PIB may be expressed as follows by substituting Eq. (A22) into Eq. (A11):

$$\mathrm{PIB} = \zeta \int_S \int_S \exp(i\phi_1) \exp^*(i\phi_2) \frac{2R J_1(\pi R l)}{l} \mathrm{d}\boldsymbol{\rho_1} \mathrm{d}\boldsymbol{\rho_2}. \quad \textbf{(A23)}$$

Funding. National Natural Science Foundation of China (NSFC) (11604327); State Key Laboratory of Applied Optics, Changchun Institute of Optics Fine Mechanics and Physics, Chinese Academy of Sciences (CAS).

REFERENCES

1. M. A. Khalighi and M. Uysal, "Survey on free space optical communication: a communication theory perspective," IEEE Commun. Surv. Tuts. **16**, 2231–2258 (2014).
2. D. O. Caplan, "Laser communication transmitter and receiver design," J. Opt. Fiber Commun. Rep. **4**, 225–362 (2007).
3. T. Weyrauch and M. A. Vorontsov, "Atmospheric compensation with a speckle beacon in strong scintillation conditions: directed energy and laser communication applications," Appl. Opt. **44**, 6388–6401 (2005).
4. A. K. Majumdar, "Free-space laser communication performance in the atmospheric channel," J. Opt. Fiber Commun. Rep. **2**, 345–396 (2005).
5. D. Killinger, "Free space optics for laser communication through the air," Opt. Photon. News **13**(10), 36–42 (2002).
6. R. K. Tyson and D. E. Canning, "Bit-error rate improvement of a laser communication system with low-order adaptive optics," in *International Symposium on Optical Science and Technology* (International Society for Optics and Photonics, 2002), pp. 82–87.
7. C. Liu, S. Chen, X. Li, and H. Xian, "Performance evaluation of adaptive optics for atmospheric coherent laser communications," Opt. Express **22**, 15554–15563 (2014).
8. C. Ruilier, *A Study of Degraded Light Coupling into Single-Mode Fibers* (Office National d'Etudes et de Recherches Aérospatiales Onera-Publications-TP, 1998).
9. J. C. Juarez, D. M. Brown, and D. W. Young, "Strehl ratio simulation results under strong turbulence conditions for actively compensated free-space optical communication systems," Proc. SPIE **8732**, 873207 (2013).
10. A. E. Siegman, "How to (maybe) measure laser beam quality," in *DPSS (Diode Pumped Solid State) Lasers: Applications and Issues* (Optical Society of America, 1998), p. MQ1.
11. F. Li, C. Geng, X. Li, and Q. Qiu, "Performance analysis of adaptive fiber laser array propagating in atmosphere with correction of high order aberrations in sub-aperture," in *International Symposium on Optoelectronic Technology and Application* (International Society for Optics and Photonics, 2016), pp. 1015414.
12. X. Ji and B. Lü, "Turbulence-induced quality degradation of partially coherent beams," Opt. Commun. **251**, 231–236 (2005).
13. D. L. Fried, "Statistics of a geometric representation of wavefront distortion," J. Opt. Soc. Am. **55**, 1427–1435 (1965).
14. L. C. Andrews and R. L. Phillips, *Laser Beam Propagation Through Random Media* (SPIE, 2005).
15. R. G. Gallager, *Principles of Digital Communication* (Cambridge University, 2008).
16. R. J. Noll, "Zernike polynomials and atmospheric turbulence," J. Opt. Soc. Am. **66**, 207–211 (1976).
17. M. Born and E. Wolf, *Principles of Optics: Electromagnetic Theory of Propagation, Interference and Diffraction of Light* (Elsevier, 2013).
18. M. Abromowitz and I. A. Stegun, "*Handbook of Mathematical Functions*," NBS (now NIST) (1965).
19. M. Reed and B. Simon, *Methods of Modern Mathematical Physics. Functional Analysis* (Academic, 1980), Vol. **1**.
20. M. A. Al-Gwaiz, *Sturm-Liouville Theory and its Applications* (Springer, 2008).
21. G. N. Watson, *A Treatise on the Theory of Bessel Functions* (Cambridge University, 1995).